BMC Oral Health

RESEARCH

Open Access

Stress distribution in angulated bendable one-piece and two-piece implant-supported single crowns in the posterior maxilla: a finite element analysis

Qassam Jaghoub[1], Çağla Yeşil[2*] and Zeynep Yeşil[1*]

Abstract

Background This finite element analysis compared stress distribution and displacement in the implant–crown complex and peri-implant bone between angulated bendable one-piece and two-piece implants supporting posterior maxillary single crowns under standardized modeling conditions.

Methods A three-dimensional finite element model of a maxillary first molar single crown in Misch bone density category 3 was generated. Two base models representing a bendable one-piece implant and a two-piece angulated implant system (15°, 4.1 × 11.5 mm) were each evaluated with 2 crown materials (monolithic zirconia and lithium disilicate) and a 0.05-mm cement layer. The bendable one-piece implant was analyzed in its final post-adjustment geometry. All component interfaces were defined as idealized bonded contacts, and a 100-N oblique load at 30° was applied to the occlusal surface in a linear static analysis.

Results Implant von Mises stresses were markedly higher in the bendable one-piece models (518–529 MPa) than in the two-piece angulated models (109–112 MPa), representing an approximately 4.7-times-higher stress level. Cement-layer stresses ranged from 22 to 29 MPa and were higher in the two-piece configurations. Crown displacement was approximately two times higher in the two-piece configurations (0.036–0.037 mm) than in the one-piece configurations (0.018 mm). Peri-implant bone principal stresses were also higher in the one-piece models, whereas differences between zirconia and lithium disilicate crowns were modest.

Conclusions Within the limitations of this finite element analysis, the two-piece angulated configuration was associated with lower implant and peri-implant bone stresses than the bendable one-piece configuration, although it showed higher cement-layer stress and crown displacement. These results represent comparative behavior within an idealized model.

Keywords Posterior maxilla, One-piece implant, Two-piece implant, Bendable implant, Abutment connection, Finite element analysis

*Correspondence:
Çağla Yeşil
cagla.yesil@erdogan.edu.tr
Zeynep Yeşil
zyesilz@hotmail.com

[1]Department of Prosthodontics, Faculty of Dentistry, Atatürk University, Erzurum 25240, Turkey
[2]Department of Prosthodontics, Faculty of Dentistry, Recep Tayyip Erdoğan University, Rize, Turkey

© The Author(s) 2026. **Open Access** This article is licensed under a Creative Commons Attribution-NonCommercial-NoDerivatives 4.0 International License, which permits any non-commercial use, sharing, distribution and reproduction in any medium or format, as long as you give appropriate credit to the original author(s) and the source, provide a link to the Creative Commons licence, and indicate if you modified the licensed material. You do not have permission under this licence to share adapted material derived from this article or parts of it. The images or other third party material in this article are included in the article's Creative Commons licence, unless indicated otherwise in a credit line to the material. If material is not included in the article's Creative Commons licence and your intended use is not permitted by statutory regulation or exceeds the permitted use, you will need to obtain permission directly from the copyright holder. To view a copy of this licence, visit http://creativecommons.org/licenses/by-nc-nd/4.0/.

Background

Osseointegrated dental implants are a predictable option for replacing missing posterior teeth and restoring function, with evidence consistently demonstrating high long-term survival for contemporary implant therapy [1–3]. However, predictable survival does not guarantee a uniform biologic and mechanical response across all clinical sites. Clinical success still depends on a balanced interaction among implant design, site-specific peri-implant bone quality, prosthetic configuration, and the direction and magnitude of functional loading transmitted to peri-implant tissues. This balance is especially challenging in the posterior maxilla, where trabecular bone is often less dense and the cortical shell relatively thin features commonly categorized as D3–D4 quality within widely used bone classifications [4]. Contemporary radiographic assessment approaches, including cone-beam computed tomography (CBCT)–derived grayscale/density estimates, indicate that implant sites in the posterior maxilla often exhibit lower mean density values than denser jaw regions, underscoring the biomechanical susceptibility of this area [5, 6]. Accordingly, biomechanical evaluation under a D3 bone scenario is clinically relevant in the posterior maxilla.

From a prosthodontic and biomechanical perspective, implant design can be broadly discussed in terms of one-piece and two-piece systems, and this difference becomes more relevant in the posterior maxilla, where bone support is often less favorable. One-piece implants integrate the abutment with the implant body, eliminating the implant–abutment junction and associated screw, which may streamline load transfer by removing a modular interface. In contrast, two-piece implants provide greater prosthetic versatility (component exchangeability and angulation correction) but introduce an implant–abutment interface that can represent a mechanically and biologically susceptible region. Clinical trials with mid-term follow-up have reported comparable outcomes for one-piece and two-piece implants supporting fixed and removable prostheses [7].

In two-piece systems, the implant–abutment interface includes a small microgap where mechanical loading and biologic responses can interact. Experimental and histologic evidence suggests that microgap-related factors and inflammatory cell infiltrates at this interface may be associated with crestal bone changes [8–10]. In vitro investigations also demonstrate measurable microleakage at the abutment–implant interface, with connection geometry influencing leakage behavior [11]. These findings align with clinical interpretations that the microgap and its position relative to the crestal bone may contribute to early marginal bone changes and should be considered in system selection and restorative planning [12]. Comparative evidence further indicates that implant–abutment connection configuration, connection geometry, and platform-switching–based restorative strategies may be associated with differences in marginal bone level outcomes after functional loading [13–15].

Bone quality and loading direction remain key determinants in implant biomechanics, particularly in low-density maxillary bone. Reviews on occlusal forces and implant biomechanics emphasize that excessive or unfavorable loading can compromise the bone–implant complex, with the crestal region and implant neck being critical areas under bending moments and oblique forces [16]. Accordingly, when comparing one-piece versus two-piece systems in a posterior maxillary molar site, it is clinically relevant to evaluate not only peri-implant bone stresses but also implant body stresses, interface-related stress concentrations, and restorative displacement.

Restorative material selection may further influence the mechanical behavior of single-unit, cement-retained implant restorations supported by one-piece or two-piece systems. Monolithic zirconia and lithium disilicate are widely used CAD/CAM ceramics with distinct elastic moduli and fracture-related properties, which may affect stress distribution across the crown, cement layer, and supporting implant components [17, 18]. The cement layer is also clinically relevant because residual excess cement has been associated with peri-implant disease, and excess cement has been identified as a potential risk indicator for peri-implant disease [19, 20]. Overall, cement- and screw-retained prostheses are generally regarded as having comparable peri-implant disease risk [21].

Finite element analysis (FEA) provides a standardized, controllable approach to compare implant–prosthesis systems under defined loading and bone-quality scenarios, enabling focused evaluation of stress/strain patterns and displacement behavior that are difficult to isolate in vivo. Despite common modeling simplifications (e.g., linear elasticity, isotropy, and idealized osseointegration), contemporary reviews conclude that comparative FEA remains valuable for hypothesis-driven assessment of how design and material variables influence load transfer in implant dentistry [22]. Published FEA has already compared one-piece and two-piece implants, and a recent study has specifically investigated different inclinations and abutment types within a bendable implant system. However, evidence remains limited for a posterior maxillary single-crown model that directly compares a bendable one-piece implant with a two-piece angulated counterpart of the same nominal dimensions and angulation while simultaneously evaluating zirconia and lithium disilicate crowns under the same D3 support and loading scenario.

Therefore, the aim of this three-dimensional finite element study was to compare the load-transfer behavior of

a bendable one-piece implant and a two-piece implant restored with monolithic zirconia or lithium disilicate cement-retained single crowns in a maxillary right first molar site (FDI 16) with D3 bone under oblique loading. Stresses in peri-implant bone, implant body, and cement layer, as well as superstructure displacement, were assessed. The study was intended as a standardized comparison of final restorative geometries under identical idealized conditions, not as a full simulation of clinical implant–abutment interface mechanics.

Null hypothesis (H0): Implant design (one-piece vs two-piece) and crown material (zirconia vs lithium disilicate) would not affect stress distribution in peri-implant bone, implant body, and cement layer, nor the displacement of the superstructure under oblique loading.

Methods

Study setting and computational environment

This finite element study followed a standardized digital workflow for geometry preparation, mesh generation, and numerical simulation. All preprocessing steps and three-dimensional (3D) analyses were performed on the same workstation (Intel Xeon E-2286, 2.40 GHz; 64 GB ECC RAM) to ensure consistency across models. Geometric modeling was performed in Blender (version 3.3; Blender Foundation, Amsterdam, the Netherlands). Meshing and preprocessing were performed in Altair HyperMesh (version 2021; Altair Engineering Inc., Troy, MI, USA), and linear static analyses were solved using a Nastran-based solver (Altair OptiStruct, version 2021; Altair Engineering Inc., Troy, MI, USA).

Anatomical source data and model generation

Maxillary bone geometry was derived from the Visible Human Project computed tomography dataset [23]. The image set (slice thickness: 0.33 mm) was imported in DICOM format into 3D Slicer [24] for reconstruction and segmentation. Threshold-based Hounsfield unit ranges were used to segment hard tissues, and the 3D anatomical structures were exported as STL files.

STL models were imported into HyperMesh and refined for analysis. A uniform cortical bone shell was generated as a 2-mm layer by applying an inward offset to the external maxillary surface, and the remaining internal volume was defined as trabecular (cancellous) bone. This two-layer representation was selected as a commonly used simplification in implant FEA [22, 25], in which bone is often modeled as a cortical shell surrounding a cancellous core; in the present study, this approach was used to enable controlled model-to-model comparisons under identical bone geometry conditions. Accordingly, the model was constructed as an idealized posterior maxillary D3 site for standardized comparative analysis, rather than as a reduced-ridge or defect-specific clinical scenario. A 3-mm mucosal layer was generated from the external maxillary surface to represent an idealized supracrestal soft-tissue envelope under standardized geometric conditions. This also ensured that the coronal bendable segment of the one-piece design remained within the supracrestal soft-tissue region. Rather than being reconstructed from patient-specific CBCT data, the mucosa was modeled as an idealized geometric layer and was not included as an outcome evaluation region. Teeth were modeled according to standard reference dental morphology. A 0.25-mm periodontal ligament (PDL) layer was generated from the external root surfaces as an idealized uniform interface to preserve standardized geometric conditions across the models. All anatomical components were then assembled within a common three-dimensional coordinate system and finalized for analysis.

Implant, restoration, and study model configurations

Implant components and restorations were modeled in Blender based on the original manufacturer-provided design data for the PROVO C (one-piece) and LEVEL (two-piece) implant systems (Mode Implant, Turkey). The evaluated implant systems are illustrated in Fig. 1a (a1–a2).

To prevent implant size from acting as a confounding factor, implant dimensions were standardized in the CAD environment (diameter: 4.1 mm; length: 11.5 mm). This diameter was selected because it was common to the compared systems and allowed direct size standardization; it was not intended to represent the default implant choice for every maxillary first molar site, where wider implants may be preferred when anatomy permits.

For the one-piece design (PROVO C), the implant body and abutment portion were modeled as a single integrated unit. The implant was placed in the maxillary right first molar site (FDI 16) with a 15° angulation. To achieve prosthetic alignment, the coronal bendable segment was modeled in its post-adjustment configuration to represent the clinically achieved restorative axis (Fig. 1b). The model represented the implant in its final post-bending geometry, whereas the intraoperative bending procedure itself was not simulated. Accordingly, bending-induced residual stress, local plastic deformation, and work-hardening effects were not captured. Subsequent analyses therefore evaluated load transfer under functional oblique loading on the final geometry only.

For the two-piece design (LEVEL), the implant and abutment were modeled as separate components forming an implant–abutment interface; screws were modeled as separate components where applicable according to the system design. The two-piece implant was placed in the maxillary right first molar site (FDI 16) with a 15° angulation and restored using a commercially available

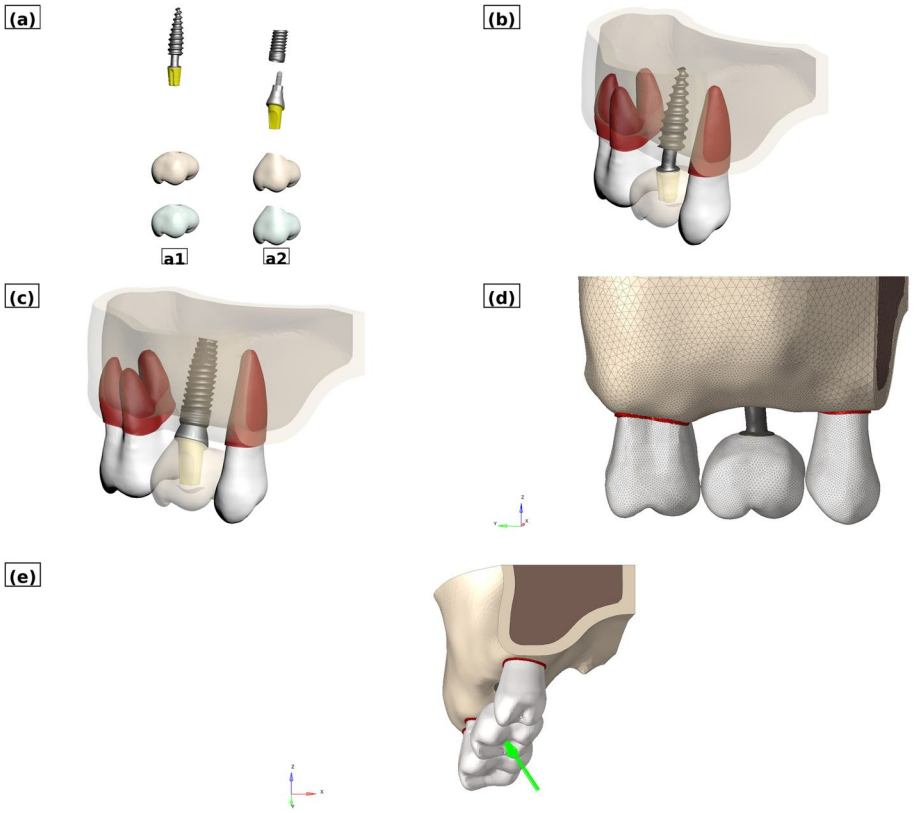


Fig. 1 Study models and loading condition: (**a**) implant systems evaluated—(a1) one-piece implant (PROVO C) and (a2) two-piece implant (LEVEL); (**b**) one-piece PROVO C implant placed at the maxillary right first molar site (FDI 16) with 15° angulation, with the coronal bendable segment adjusted to realign the prosthetic axis; (**c**) two-piece LEVEL implant placed at site FDI 16 with 15° angulation and restored with a 15° angled cement-retained abutment; (**d**) finite element mesh of the assembled implant–abutment–restoration complex and surrounding structures; (**e**) loading configuration showing a 100-N oblique force applied at 30° to the long axis of the implant in the bucco-palatal direction to the restoration central fossa

Table 1 Base finite element models and corresponding crown-material configurations

Base model	Implant system	Crown-material configuration
M1	Mode PROVO C (one-piece)	Zirconia; Lithium disilicate
M2	Mode LEVEL (two-piece)	Zirconia; Lithium disilicate

15° angled cement-retained abutment (Fig. 1c). This abutment was selected to standardize the comparator within the evaluated system; customized CAD/CAM abutments were outside the scope of the present study.

A uniform 0.05-mm resin cement layer was modeled between the inner surface of the crown and the supporting abutment surface in both systems (the separate abutment in the two-piece design and the integrated abutment portion in the one-piece design), representing an ideal cementation scenario consistent with commonly used thin cement-film assumptions in implant FEA workflows [26, 27]. Prior to analysis, mesh compatibility and interface conformity operations were performed to ensure appropriate load transfer across assembled components.

Two base finite element models were generated according to implant system: M1 represented the PROVO C one-piece design and M2 represented the LEVEL two-piece design. Each base model was then analyzed with two superstructure materials (zirconia and lithium disilicate), yielding four simulation configurations.The two base models and their crown-material configurations are summarized in Table 1.

Finite element meshing, solver, and convergence assessment

After completion of geometric modeling, all components were meshed in HyperMesh. Surface meshes were generated using triangular elements with a target size range of 0.05–0.25 mm, and solid meshes were generated using tetrahedral elements. Mesh convergence (mesh independence) was evaluated using progressively refined meshes until the change in peak stress values at clinically relevant regions (peri-implant crestal cortical bone and implant neck regions) was within 5% between successive refinements. Additionally, the change in total strain energy

between the final two mesh densities was < 0.1%, consistent with commonly reported implant FEA verification approaches [27]. A representative finite element mesh of the assembled model is shown in Fig. 1d. The assembled FEMs were exported to OptiStruct (Altair Engineering, Inc., Troy, MI, USA), and linear static analyses were performed.

Material properties

All materials were assumed to be homogeneous, isotropic, and linearly elastic. Young's modulus (E) and Poisson's ratio (ν) used in the analyses are listed in Table 2. The elastic moduli for cortical bone (13,700 MPa) and trabecular bone (1,370 MPa) were selected to represent D3 bone quality as defined by the Misch classification [4] and were supported by experimental biomechanical measurements of bone elastic properties [28]. Material properties for titanium, resin cement, zirconia, and lithium disilicate were adopted from commonly used dental biomechanics and all-ceramic materials literature [27, 29, 30].

Contact definitions and interface assumptions

All component interfaces were defined as idealized tied (bonded) contacts (OptiStruct "FREEZE"), including complete osseointegration at the bone–implant interface and ideal adhesion at the cement–abutment and cement–crown interfaces. This strategy ensured consistent boundary conditions across models and allowed isolation of the effects of implant configuration and restorative material on load transfer. Because implant–abutment microgap behavior, frictional contact, and abutment screw preload were not simulated, the two-piece system was treated as an idealized assembly with reduced interface compliance. Accordingly, the analysis focused on comparative stress distribution and displacement in the final restorative geometries, whereas preload-dependent stiffness, micromovement, and interface separation were outside the scope of the present model.

Table 2 Material properties used in the analyses

Material	Young's Modulus (MPa)	Poisson's Ratio
Cortical bone	13,700	0.30
Trabecular bone	1,370	0.30
Titanium	110,000	0.35
Tooth structure	19,600	0.30
Periodontal ligament (PDL)	0.69	0.45
Resin cement	8,000	0.33
Zirconia	200,000	0.31
Lithium disilicate	95,000	0.23

Loading scenario and boundary conditions

All simulations were performed as linear static analyses. This approach was chosen to establish a controlled baseline comparison across model configurations, but it does not capture nonlinear contact behavior, preload-dependent stiffness, material yielding, or fatigue accumulation.

A 100-N oblique load was applied at 30° to the long axis of the implant in the bucco-palatal direction to the central fossa of the restoration [31]. To reduce stress singularities at the load application site, the load was distributed across nodes within an approximately 1-mm-diameter area. The load direction and application site are illustrated in Fig. 1e. This loading scenario was selected to provide a standardized non-axial loading condition for comparison between model configurations.

For boundary conditions, nodes located in the superior region of the maxillary bone were fully constrained by restricting translational degrees of freedom in the x, y, and z directions. A global Cartesian coordinate system was established with the x-axis oriented bucco-palatal, the y-axis mesio-distal, and the z-axis supero-inferior. Under the specified loading and boundary conditions, four linear static analyses were performed.

Model size, outcome variables, and model verification

Model sizes were as follows: M1 (one-piece) included 175,217 nodes and 674,711 elements, whereas M2 (two-piece) included 310,005 nodes and 1,196,498 elements. Outcome measures included minimum and maximum principal stresses (σmin and σmax) in peri-implant bone, von Mises stress (σvM) in the implant and resin cement layer, and maximum resultant displacement of the superstructure. Peak values and stress/displacement distributions were compared between models to identify relative differences in mechanical behavior. Because each model represented a deterministic numerical simulation rather than repeated experimental measurements, comparisons were descriptive and no inferential statistical tests were applied. The biomechanical outcomes evaluated in the present study are summarized in Table 3.

Although experimental validation was beyond the scope of this study, the modeling workflow, mesh refinement strategy, and analysis assumptions were aligned with commonly reported implant FEA methodologies [27]. In addition, stress distribution patterns were qualitatively checked against those reported in prior computational studies employing comparable non-axial loading conditions to confirm consistency with established biomechanical principles [31].

Results

The biomechanical outcomes of the two finite element models under the specified oblique loading condition are summarized in Table 3. Overall, implant design produced

Table 3 Biomechanical outcomes of the two finite element models under 100-N oblique loading (30°) at the maxillary first molar site

Model	Implant System (Design)	Crown Material	Bone σmin (MPa)	Bone σmax (MPa)	Implant σvM (MPa)	Cement σvM (MPa)	Superstructure Displacement (mm)
M1	PROVO C (one-piece)	Zirconia	−71.946	25.012	518.240	24.487	0.01789
M1	PROVO C (one-piece)	Lithium disilicate	−73.414	25.522	528.820	22.364	0.01793
M2	LEVEL (two-piece)	Zirconia	−55.447	22.657	109.264	29.414	0.03611
M2	LEVEL (two-piece)	Lithium disilicate	−56.646	23.097	111.629	26.782	0.03694

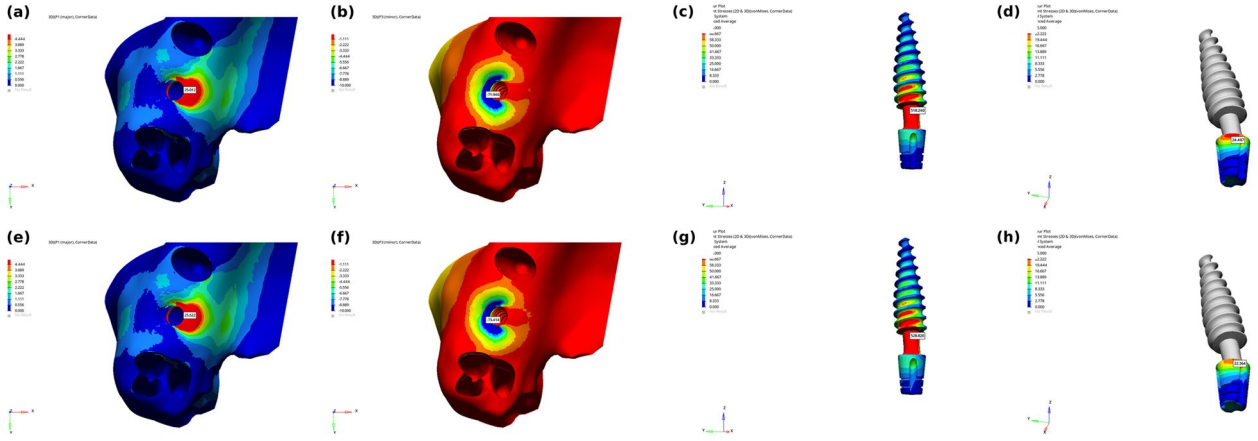


Fig. 2 Finite element stress distribution results for Model M1 with different restorative materials: zirconia (**a**-**d**) and lithium disilicate (**e**-**h**). **a**, **e** maximum principal stress in peri-implant bone; (**b**, **f**) minimum principal stress in peri-implant bone; (**c**, **g**) von Mises stress in the implant; and (**d**, **h**) von Mises stress in the resin cement layer. Within each outcome category, identical color-scale ranges were applied to facilitate direct visual comparison between the restorative-material configurations

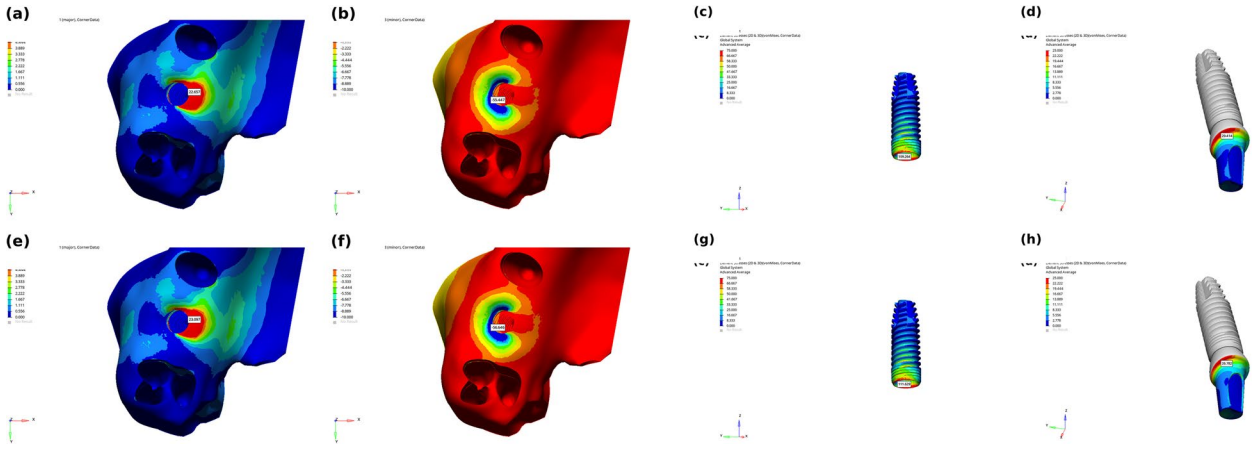


Fig. 3 Finite element stress distribution results for Model M2 with different restorative materials: zirconia (**a**-**d**) and lithium disilicate (**e**-**h**). **a**, **e** maximum principal stress in peri-implant bone; (**b**, **f**) minimum principal stress in peri-implant bone; (**c**, **g**) von Mises stress in the implant; and (**d**, **h**) von Mises stress in the resin cement layer. Within each outcome category, identical color-scale ranges were applied to facilitate direct visual comparison between the restorative-material configurations

the dominant differences between models, with the one-piece model (M1), across both crown materials, showing higher peri-implant bone principal stresses and markedly higher implant von Mises stresses, whereas the two-piece model (M2), across both crown materials, exhibited greater cement-layer stress and superstructure displacement. Descriptive relative differences are reported below. Stress contour maps are presented for Model M1 in Fig. 2 and for Model M2 in Fig. 3, and superstructure displacement for all configurations is shown in Fig. 4.

Bone principal stresses

Peri-implant bone principal stresses were consistently higher in the one-piece model than in the two-piece

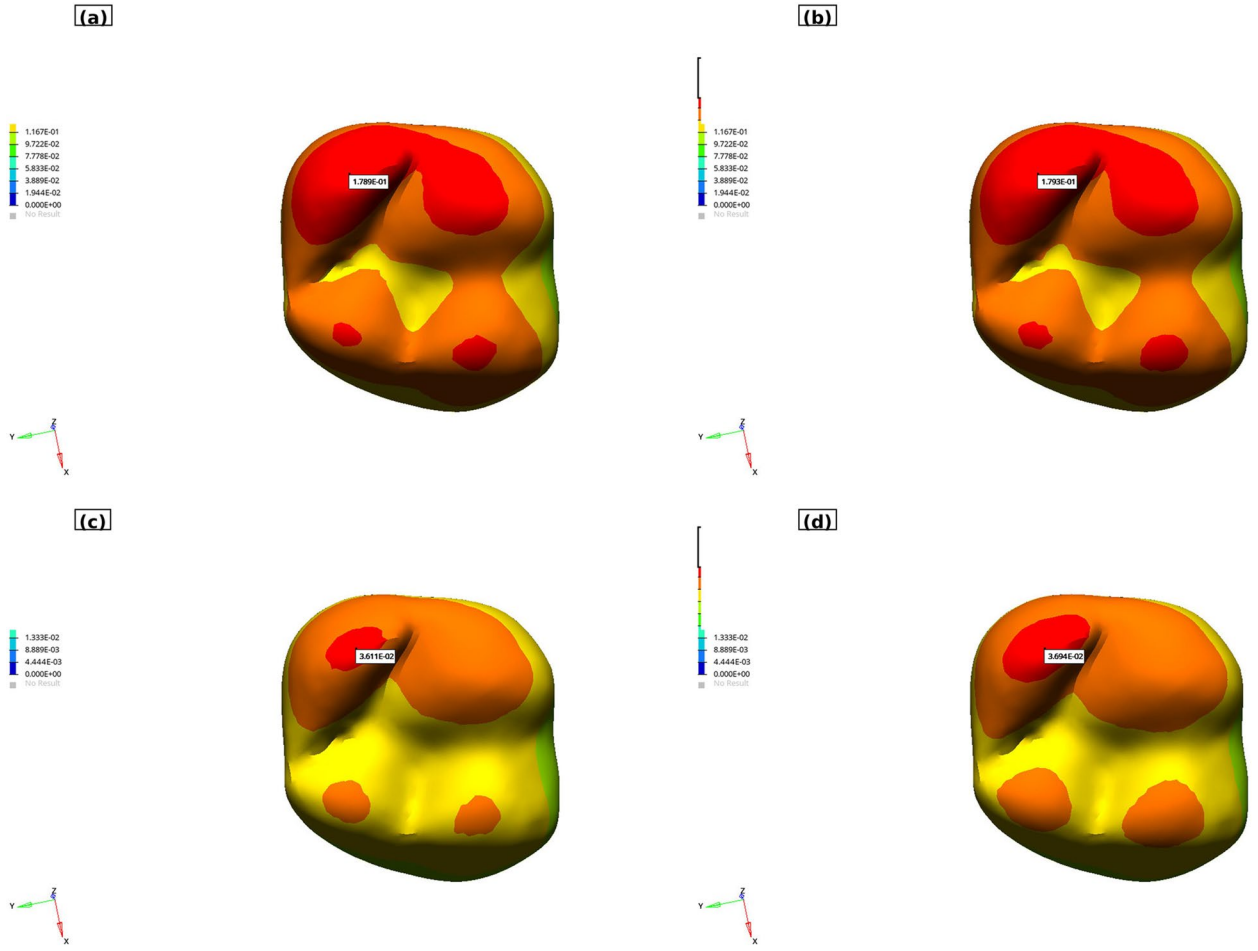


Fig. 4 Total displacement distributions under the applied loading condition: (**a**) Model M1 with zirconia, (**b**) Model M1 with lithium disilicate, (**c**) Model M2 with zirconia, and (**d**) Model M2 with lithium disilicate. Within each outcome category, identical color-scale ranges were applied to facilitate direct visual comparison between the restorative-material configurations

model under both crown materials (Table 3; Figs. 2 and 3). Compressive stresses (σmin) ranged from – 55.447 to – 73.414 MPa. The magnitude of peak compression was approximately 30% higher in the one-piece model than in the matched two-piece configuration, with the highest compression observed in the lithium disilicate-restored one-piece configuration. Tensile stresses (σmax) ranged from 22.657 to 25.522 MPa and were approximately 10% higher in the one-piece model. Within each implant design, lithium disilicate produced only slight increases in bone principal stress relative to zirconia.

Implant and cement von Mises stresses

Implant von Mises stress (σvM) exhibited the largest between-model differences (Table 3; Figs. 2 and 3). The one-piece model demonstrated substantially higher implant σvM under both crown materials (518.240–528.820 MPa) than the two-piece model (109.264–111.629 MPa), corresponding to an approximately 4.7-fold increase. Cement-layer σvM ranged from 22.364 to 29.414 MPa. In contrast to the implant body, cement-layer stresses were higher in the two-piece configurations by approximately 20%, with the highest cement σvM observed in the zirconia-restored two-piece configuration and the lowest value in the lithium disilicate-restored one-piece configuration.

Superstructure displacement

Maximum resultant displacement of the superstructure ranged from 0.01789 to 0.03694 mm (Table 3; Fig. 4). The two-piece models showed approximately two-fold higher displacement (≈0.036–0.037 mm) than the one-piece models (≈0.018 mm), demonstrating reduced overall rigidity of the two-piece implant–abutment–restoration assembly under the present idealized conditions. Within each implant design, the effect of crown material on displacement was negligible compared with the effect of implant design.

Discussion

This finite element study compared angulated bendable one-piece and two-piece implant-supported single crowns in an idealized posterior maxillary D3 model. The main finding was that implant configuration dominated the mechanical response under the applied oblique load: the one-piece design generated higher implant and peri-implant bone stresses, whereas the two-piece design showed greater cement-layer stress and superstructure displacement. By contrast, the influence of crown material was comparatively small. Accordingly, the null hypothesis was rejected for implant configuration, while only a modest effect of crown material was identified within the standardized assumptions of the present analysis. These results should be interpreted as comparative load-transfer patterns of the final restorative geometries under bonded-contact conditions rather than as a full representation of true clinical one-piece versus two-piece interface mechanics.

A 100-N oblique load applied at 30° to the implant long axis was selected to represent a conservative functional mastication scenario rather than extreme clenching. Reported masticatory forces during functional activities commonly fall within approximately 74–167 N, supporting 100 N as a physiologic reference level for comparative modeling [32]. This loading magnitude and angulation are consistent with commonly used implant FEA protocols for evaluating non-axial load transfer under standardized conditions [33, 34]. Implant diameter and length were standardized across designs to control macro-geometry and minimize dimensional confounding, thereby enabling a more valid comparison of the two implant concepts under identical size conditions. The selected 4.1-mm diameter reflects a standardized system-specific comparison rather than a claim that this dimension is the preferred choice for all maxillary first molar sites. Because implant dimensions can independently affect peri-implant biomechanics, larger diameters and, to a lesser extent, longer implants have been associated with lower crestal stress/strain concentrations by increasing the load-bearing area and reducing bending effects [35, 36].

A D3 bone scenario was selected to represent reduced-density posterior maxillary support as described in widely used classifications and to enable controlled comparisons under a clinically relevant support condition [37]. Prior FEAs similarly show that bone quality can meaningfully influence stress distribution patterns in implant-supported restorations, particularly under non-axial loading conditions [38, 39]. At the same time, the present model should not be interpreted as a reduced-ridge or compromised-volume anatomy specifically indicating narrow implants; rather, it is an idealized support condition used to hold bone geometry constant across models.

A uniform 0.05-mm (50-μm) resin cement film was modeled to permit comparison of the luting layer under controlled conditions, and cement-layer σvM was evaluated. In implant crown simulations, increasing cement-film thickness has been associated with higher and more cervically concentrated stresses within the luting layer [40]. From a clinical standpoint, cement-film characteristics and luting-agent selection are also considered relevant variables in fixed prosthodontics [41]. Implant FEAs further indicate that prosthetic interface assumptions and connection geometry can influence stress patterns under non-axial loading [42]. In the present models, the two-piece configuration reduced implant stress but shifted relatively higher stress toward the cement layer, suggesting a redistribution of load within the restorative assembly under the adopted assumptions.

Under identical oblique loading, the one-piece implant design with a bendable coronal segment produced higher compressive peri-implant bone stresses and markedly higher implant von Mises stresses than the two-piece design. This pattern is broadly consistent with previous finite element and experimental comparisons in which one-piece or narrower implants showed less favorable stress concentrations under non-axial loading than selected two-piece alternatives [43, 44].

The present results are partly in line with a recent finite element analysis comparing one-piece and two-piece implants, which found lower cortical bone stresses in the two-piece model but lower crown-body stresses in the one-piece model [45]. Similarly, in the present study, the bendable one-piece design generated higher peri-implant bone and implant stresses, whereas the two-piece design showed higher cement-layer stress and greater superstructure displacement. These combined findings indicate that no single implant concept appears uniformly advantageous across all biomechanical outcomes; rather, the observed response depends on the component or tissue assessed and on the specific modeling assumptions.

Within the same implant design, lithium disilicate resulted in slightly higher tensile and compressive principal stresses in the peri-implant bone than zirconia in the present models, and the effect of crown material remained modest compared with the effect of implant design. Similar material-dependent differences have been reported in three-dimensional finite element studies evaluating implant-supported single crowns, where changes in restorative stiffness were associated with modest shifts in peri-implant stress metrics under non-axial loading [46, 47]. Overall, these reports support that crown material can influence stress transfer patterns, although the magnitude of this effect is typically secondary to the effects of implant design and loading conditions.

Peak implant stresses in the one-piece models (518–529 MPa) were substantially higher than those in the two-piece models; however, they remained below the reported yield strength (approximately 795 MPa) and ultimate tensile strength (approximately 900 MPa) of Ti-6Al-4 V [48]. This comparison should nevertheless be interpreted cautiously, because the implant material was represented using a simplified linear-elastic assumption based on elastic modulus and Poisson's ratio, rather than a full material model incorporating nonlinear or fatigue behavior. Even so, the findings indicate a smaller mechanical safety margin for the one-piece configuration under the present loading condition than for the two-piece configuration.

Superstructure displacement was higher in the two-piece configurations, while zirconia tended to reduce displacement relative to lithium disilicate within the same implant design. This pattern is consistent with evidence that multi-component implant–abutment assemblies exhibit measurable compliance and that abutment micromovement can vary according to connection characteristics [49]. From a material perspective, simulations across implant-supported prosthetic materials indicate lower deformation in stiffer restorative systems under comparable loading [50]. A commercially available 15° stock abutment was selected here to standardize the comparator; customized CAD/CAM abutments, which may alter stress transfer, warrant dedicated future study [42]. Direct clinical corroboration of the present findings remains limited because available comparative studies have been conducted in different treatment contexts. In an esthetic-zone clinical trial, one-piece and two-piece abutments supporting single crowns were considered equivalent with respect to peri-implant esthetics, patient satisfaction, and oral health-related quality of life [51]. Because that study differed from the present posterior maxillary single-crown model in implant/abutment configuration, anatomical site, and loading context, it should be regarded as indirect clinical context rather than direct validation of the current findings.

Several limitations should be acknowledged. The implant–abutment interface in the two-piece model was simplified as a bonded connection without screw preload or friction, which does not reproduce microgap formation, interface slip, or preload-dependent stiffness and may therefore overestimate the rigidity of the assembly. Likewise, the bendable one-piece implant was evaluated only in its final post-adjustment geometry, whereas the bending procedure itself and any associated residual stress or local plastic deformation were not simulated. The bone model was further simplified as a homogeneous, isotropic, linearly elastic D3 structure with a uniform 2-mm cortical layer and complete osseointegration, allowing standardized comparison but not reflecting patient-specific anatomical and material variability. The loading condition was restricted to a single static 100-N oblique force, and more complex cyclic or multidirectional loading scenarios were beyond the scope of the present model. In addition, the comparison was standardized using a 4.1-mm implant diameter and a stock 15° cement-retained abutment; different diameters or customized abutment designs may lead to different biomechanical responses. These factors should be addressed in future studies incorporating more anatomically realistic geometries, preload-dependent interface modeling, and cyclic loading conditions.

Conclusions

Within the limitations of the present finite element study, implant design was the primary determinant of the observed mechanical response in posterior maxillary single-crown restorations. The bendable one-piece configuration showed higher implant and peri-implant bone stresses, whereas the two-piece configuration showed higher cement-layer stress and greater displacement. Crown material produced comparatively small changes within each implant design. These findings help characterize comparative load-transfer tendencies of the evaluated final geometries; however, they should not be interpreted as direct evidence of clinical interface mechanics or long-term failure risk without further validation under more detailed mechanical conditions.

Abbreviations

CAD/CAM	Computer-aided design/computer-aided manufacturing
CBCT	Cone-beam computed tomography
DICOM	Digital Imaging and Communications in Medicine
ECC	Error-correcting code
FDI	Fédération Dentaire Internationale
FEA	Finite element analysis
PDL	Periodontal ligament
RAM	Random access memory
STL	Stereolithography

Acknowledgements

The authors gratefully acknowledge Mode Implant (Istanbul, Turkey) for providing implant model files and relevant design specifications that enabled accurate three-dimensional model construction. The authors also thank Tinus Technologies (Ankara, Turkey) for professional technical support, including implementation and execution of the finite element analysis workflow. The authors further acknowledge the Recep Tayyip Erdoğan University Development Foundation for supporting the open access publication of this article.

Authors' contributions

Conceptualization: QJ, ZY; Methodology: QJ, CY, ZY; Software/FEA workflow: QJ, CY; Formal analysis: QJ, CY; Writing—original draft: QJ, CY, ZY; Writing—review & editing: QJ, CY, ZY; Supervision: ZY. All authors read and approved the final manuscript.

Funding

Open access / article processing charge (APC) support for this article was provided by the Recep Tayyip Erdoğan University Development Foundation (Grant No. 0202600424278).

Data availability
The datasets generated and/or analysed during the current study are available from the corresponding author on reasonable request.

Declarations

Ethics approval and consent to participate
Not applicable (in this silico finite element analysis; no human or animal participants).

Consent for publication
Not applicable.

Competing interests
The authors declare no competing interests.

Received: 7 February 2026 / Accepted: 16 April 2026
Published online: 20 May 2026

References

1. Howe MS, Keys W, Richards D. Long-term (10-year) dental implant survival: a systematic review and sensitivity meta-analysis. J Dent. 2019;84:9–21.
2. Pjetursson BE, Thoma D, Jung R, Zwahlen M, Zembic A. A systematic review of the survival and complication rates of implant-supported fixed dental prostheses after a mean observation period of at least 5 years. Clin Oral Implants Res. 2012;23(Suppl 6):22–38.
3. Jung RE, Pjetursson BE, Glauser R, Zembic A, Zwahlen M, Lang NP. A systematic review of the 5-year survival and complication rates of implant-supported single crowns. Clin Oral Implants Res. 2008;19(2):119–30.
4. Misch CE. Contemporary Implant Dentistry. 3rd ed. St Louis (MO): Mosby Elsevier; 2008.
5. Hao Y, Zhao W, Wang Y, Yu J, Zou D. Assessments of jaw bone density at implant sites using 3D cone-beam computed tomography. Eur Rev Med Pharmacol Sci. 2014;18(9):1398–403.
6. Reeves TE, Mah P, McDavid WD. Deriving Hounsfield units using grey levels in cone beam CT: a clinical application. Dentomaxillofac Radiol. 2012;41(6):500–8.
7. Gamper FB, Benic GI, Sanz-Martin I, Asgeirsson AG, Hämmerle CHF, Thoma DS. Randomized controlled clinical trial comparing one-piece and two-piece dental implants supporting fixed and removable dental prostheses: 4- to 6-year observations. Clin Oral Implants Res. 2017;28(12):1553–9.
8. Hermann JS, Schoolfield JD, Schenk RK, Buser D, Cochran DL. Influence of the size of the microgap on crestal bone changes around titanium implants: A histometric evaluation of unloaded non-submerged implants in the canine mandible. J Periodontol. 2001;72(10):1372–83.
9. Broggini N, McManus LM, Hermann JS, Medina RU, Oates TW, Schenk RK, et al. Persistent acute inflammation at the implant-abutment interface. J Dent Res. 2003;82(3):232–7.
10. Broggini N, McManus LM, Hermann JS, Medina R, Schenk RK, Buser D, et al. Peri-implant inflammation defined by the implant-abutment interface. J Dent Res. 2006;85(5):473–8.
11. Larrucea Verdugo C, Jaramillo Núñez G, Acevedo Avila A, Larrucea San Martín C. Microleakage of the prosthetic abutment/implant interface with internal and external connection: In vitro study. Clin Oral Implants Res. 2014;25(9):1078–83.
12. Schwarz F, Hegewald A, Becker J. Impact of implant-abutment connection and positioning of the machined collar/microgap on crestal bone level changes: a systematic review. Clin Oral Implants Res. 2014;25(4):417–25.
13. Caricasulo R, Malchiodi L, Ghensi P, Fantozzi G, Cucchi A. The influence of implant-abutment connection to peri-implant bone loss: a systematic review and meta-analysis. Clin Implant Dent Relat Res. 2018;20(4):653–64.
14. Camps-Font O, Rubianes-Porta L, Valmaseda-Castellón E, Jung RE, Gay-Escoda C, Figueiredo R. Comparison of external, internal flat-to-flat, and conical implant abutment connections for implant-supported prostheses: a systematic review and network meta-analysis of randomized clinical trials. J Prosthet Dent. 2023;130(3):327–40.
15. Juan-Montesinos A, Agustín-Panadero R, Solá-Ruiz MF, Marco-Pitarch R, Montiel-Company JM, Fons-Badal C. Comparative study by systematic review and meta-analysis of the peri-implant effect of two types of platforms: Platform-switching versus conventional platforms. J Clin Med. 2022;11(6):1743.
16. Isidor F. Influence of forces on peri-implant bone. Clin Oral Implants Res. 2006;17(Suppl 2):8–18.
17. Zarone F, Di Mauro MI, Ausiello P, Ruggiero G, Sorrentino R. Current status on lithium disilicate and zirconia: a narrative review. BMC Oral Health. 2019;19(1):134.
18. Denry I, Kelly JR. State of the art of zirconia for dental applications. Dent Mater. 2008;24(3):299–307.
19. Wilson TG Jr. The positive relationship between excess cement and peri-implant disease: a prospective clinical endoscopic study. J Periodontol. 2009;80(9):1388–92.
20. Staubli N, Walter C, Schmidt JC, Weiger R, Zitzmann NU. Excess cement and the risk of peri-implant disease: a systematic review. Clin Oral Implants Res. 2017;28(10):1278–90.
21. Reis INRD, Fukuoka GL, Nagay BE, Pannuti CM, Spin-Neto R, da Silva EVF. Incidence of peri-implant disease associated with cement- and screw-retained implant-supported prostheses: a systematic review and meta-analysis. J Prosthet Dent. 2025;134(1):100–8.
22. Falcinelli C, Valente F, Vasta M, Traini T. Finite element analysis in implant dentistry: state of the art and future directions. Dent Mater. 2023;39(6):539–56.
23. Spitzer VM, Whitlock DG. The visible human dataset: the anatomical platform for human simulation. Anat Rec. 1998;253(2):49–57.
24. Fedorov A, Beichel R, Kalpathy-Cramer J, Finet J, Fillion-Robin JC, Pujol S, et al. 3D Slicer as an image computing platform for the Quantitative Imaging Network. Magn Reson Imaging. 2012;30(9):1323–41.
25. Paracchini L, Barbieri C, Redaelli M, Di Croce D, Vincenzi C, Guarnieri R. Finite element analysis of a new dental implant design optimized for the desirable stress distribution in the surrounding bone region. Prosthesis. 2020;2(3):225–36.
26. Özdogan MS, Gökçe H. Investigation of the effects of cement in different thicknesses and mechanical properties on implant with zirconia crown: a finite element analysis. J Int Oral Health. 2020;12(5):491–7.
27. Geng JP, Tan KB, Liu GR. Application of finite element analysis in implant dentistry: a review of the literature. J Prosthet Dent. 2001;85(6):585–98.
28. Rho JY, Ashman RB, Turner CH. Young's modulus of trabecular and cortical bone material: ultrasonic and microtensile measurements. J Biomech. 1993;26(2):111–9.
29. Raigrodski AJ. Contemporary materials and technologies for all-ceramic fixed partial dentures: a review of the literature. J Prosthet Dent. 2004;92(6):557–62.
30. Zupancic Cepic L, Frank M, Reisinger A, Pahr D, Zechner W, Schedle A, et al. Biomechanical finite element analysis of short-implant-supported, 3-unit, fixed CAD/CAM prostheses in the posterior mandible. Int J Implant Dent. 2022;8:8.
31. Oliveira H, Brizuela Velasco A, Ríos-Santos JV, Sánchez Lasheras F, Lemos BF, Gil FJ, et al. Effect of different implant designs on strain and stress distribution under non-axial loading: a three-dimensional finite element analysis. Int J Environ Res Public Health. 2020;17(13):4738.
32. Poli O, Manzon L, Niglio T, Ettorre E, Vozza I. Masticatory force in relation with age in subjects with full permanent dentition: a cross-sectional study. Healthcare (Basel). 2021;9(6):700.
33. Lee JH, Jang HY, Lee SY. Finite element analysis of dental implants with zirconia crown restorations: conventional cement-retained vs cementless screw-retained. Materials (Basel). 2021;14(10):2666.
34. Oh JH, Kim YS, Lim JY, Choi BH. Stress distribution on the prosthetic screws in the All-on-4 concept: a three-dimensional finite element analysis. J Oral Implantol. 2020;46(1):3–12.
35. Himmlová L, Dostálová T, Kácovský A, Konvicková S. Influence of implant length and diameter on stress distribution: a finite element analysis. J Prosthet Dent. 2004;91(1):20–5.
36. Petrie CS, Williams JL. Comparative evaluation of implant designs: Influence of diameter, length, and taper on strains in the alveolar crest. A three-dimensional finite-element analysis. Clin Oral Implants Res. 2005;16(4):486–94.
37. Misch CE. Dental Implant Prosthetics. 2nd ed. St Louis (MO): Mosby/Elsevier; 2014.
38. Ulu M, Yasin M, Şahin O, Akçay H. A finite element analysis to study the stress distribution on distal implants in All-on-Six treatment concepts as affected tilted and short implant. J Oral Implantol. 2024;50(3):245–53.
39. Sevimay M, Turhan F, Kiliçarslan MA, Eskitascioglu G. The effect of different bone qualities on stress distribution in an implant-supported crown: a three-dimensional finite element analysis. J Prosthet Dent. 2005;93(3):227–34.

40. Ha SR, Kim SH, Lee JB, Han JS, Yeo IS, Yoo SH, et al. Biomechanical three-dimensional finite element analysis of monolithic zirconia crown with different cement thickness. Ceram Int. 2016;42(13):14928–36.
41. Diaz-Arnold AM, Vargas MA, Haselton DR. Current status of luting agents for fixed prosthodontics. J Prosthet Dent. 1999;81:135–41.
42. Ziada A, Beleidy M. Influence of different customized abutment materials on stress distribution of different internal implant-abutment connections: finite element analysis. BMC Oral Health. 2025;25(1):82.
43. Wu AYJ, Hsu JT, Chee W, Lin YT, Fuh LJ, Huang HL. Biomechanical evaluation of one-piece and two-piece small-diameter dental implants: in-vitro experimental and three-dimensional finite element analyses. J Formos Med Assoc. 2016;115(9):794–800.
44. Barbosa FT, Zanatta LCS, de Souza RE, Gehrke SA. Comparative analysis of stress distribution in one-piece and two-piece implants with narrow and extra-narrow diameters: a finite element study. PLoS One. 2021;16(2):e0245800.
45. Mohamed NAA, El-Zawahry MM, El-Anwar M, Hussein HAH. One-piece versus two-piece dental implants. Ahram Can Dent J. 2025;4(2):123–33.
46. Valente F, Marrocco A, Falcinelli C. Impact of physiological and non-physiological loading scenarios and crown material on periimplant bone stress distribution: a 3D finite element study. J Mech Behav Biomed Mater. 2025;163:106894.
47. El-Anwar MI, Al-Azrag KE, Ghazy MH, Dawood LE. Influence of implant-abutment angulations and crown material on stress distribution on central incisor: a 3D FEA. Braz J Oral Sci. 2015;14(4):323–9.
48. Nicholson JW. Titanium alloys for dental implants: a review. Prosthesis. 2020;2(2):100–16.
49. Yamanishi Y, Yamaguchi S, Imazato S, Nakano T, Yatani H. Influences of implant neck design and implant-abutment joint type on peri-implant bone stress and abutment micromovement: three-dimensional finite element analysis. Dent Mater. 2012;28(11):1126–33.
50. Hazir Y, Aktas S, Dundar S, Kocyigit ID, Cakmak G, Yildirim TT, et al. Biomechanical behavior of titanium, cobalt-chromium, zirconia, and PEEK frameworks in implant-supported prostheses: a dynamic finite element analysis. BMC Oral Health. 2025;25(1):97.
51. Pascoal ALB, Paiva KRG, de Araujo LNM, Marinho LCN, Gurgel BCV, Dantas WRM, et al. One-piece versus two-piece abutments for single crowns in the esthetic zone: a clinical trial. Clin Oral Implants Res. 2025;36(2):143–52.

Publisher's Note

Springer Nature remains neutral with regard to jurisdictional claims in published maps and institutional affiliations.